

Ellipsoidal Variability in the OGLE Planetary Transit Candidates

E. Sirko & B. Paczyński

Princeton University Observatory, Princeton, NJ 08544-1001, USA

E-mail: esirko@astro.princeton.edu

E-mail: bp@astro.princeton.edu

ABSTRACT

We analyze the photometry of 117 OGLE stars with periodic transit events for the presence of ellipsoidal light variations, which indicate the presence of massive companions. We find that $\sim 50\%$ of objects may have stellar companions, mostly among the short period systems. In our Table 1 we identify a coefficient of ellipsoidal variability for each star, a_{e2} , which can be used to select prime candidates for planetary searches. There is a prospect of improving the analysis, and the systems with smaller ellipsoidal variability will be identified, when the correlations in the OGLE photometry are corrected for in the future, thereby providing a cleaner list of systems with possible planets.

Subject headings: planetary systems – surveys – techniques: photometric

1. Introduction

The first extra solar planet discovered to exhibit photometric transits was HD 209458 (Charbonneau et al. 2000, Henry et al. 2000), but its orbit had been first determined spectroscopically (Mazeh et al. 2000). Massive efforts to detect photometric transits on their own put at least 23 teams into the competition (Horne 2003). By far the largest list of periodic transit candidates was published by the OGLE team (Udalski et al. 2002a,b,c), with a total of 121 objects, with all photometric data available on the Web. The first confirmation that at least one of these has a ‘hot Jupiter’ planet was obtained by Konacki et al. (2003). They also found that a large fraction of OGLE candidates were ordinary eclipsing binaries blended with a brighter star which was not variable, and its light diluted the depth of the eclipses, so they appeared as shallow transits.

It was clear from the beginning that many transits may be due to red dwarfs or brown dwarfs, and that some of these massive companions may give rise to ellipsoidal light variability (Udalski et al. 2002a). In fact in that paper OGLE-TR-5 and OGLE-TR-16 were

noted to exhibit such a variability, indicating that the companion mass had to be substantial. Ellipsoidal variability is a well known phenomenon among binary stars (cf. Shobbrook et al. 1969, and references therein). Tidal effects are responsible for making a star elongated toward the companion. Ellipsoidal variability is due to the changes in the angular size of the distorted star and to gravity darkening, with half of the orbital period. Obviously, the more massive the companion, and the closer it is to the primary, the stronger the effect. It can be used to remove from the OGLE sample objects which have massive, and therefore not planetary, companions (Drake 2003).

The aim of this paper is to extend the work of Drake (2003) to the new list of OGLE transit candidates (Udalski 2002c) and to provide a more realistic error analysis, which is needed in order to assess the reality of ellipsoidal variability.

2. Data Analysis

We took all photometric data from the OGLE Web site:

<http://sirius.astro.uw.edu.pl/~ogle/>

<http://bulge.princeton.edu/~ogle/>

There are three data sets: two provide a total of 59 objects in the field close to the Galactic Center (Udalski et al. 2002a,b), and the third provides 62 objects in a field in the Galactic Disk in Carina (Udalski et al. 2002c). There are typically 800 data points for OGLE-TR-1 - OGLE-TR-59, and 1,150 data points for OGLE-TR-60 - OGLE-TR-121. The Carina data set had somewhat longer exposures and the field was much less crowded, so the photometric accuracy is somewhat better than in the Galactic Center field.

To analyze the light curves for ellipsoidal variability the data points within the transits must first be removed. Our algorithm was to start at mid-transit, working outwards, and to reject data points until the third data point for which the baseline magnitude was within its photometric error bars. We then obtained a five parameter fit to the rest of the data:

$$I_k = \langle I \rangle + a_{c1} \cos p_k + a_{s1} \sin p_k + a_{c2} \cos 2p_k + a_{s2} \sin 2p_k, \quad (1)$$

where I_k is data point number k , and p_k is its phase calculated with the orbital period provided by Udalski et al. (2002a,b,c). The phase is $p = 0$ at mid transit. The values of all five parameters: $\langle I \rangle$, a_{c1} , a_{s1} , a_{c2} , and a_{s2} were calculated with a least squares method. The formal errors for all the sinusoidal coefficients for a given star were practically the same. Fig. 1 shows period-folded light curves of several objects, with the best-fit five-parameter function (eq. 1) over plotted. Ellipsoidal variability is clearly visible in objects such as

OGLE-TR-16 as a sinusoidal component with half the period of the binary and with the phase of minimum light flux being the same as the phase of the transit.

In the five parameter fit given with eq. (1) the term a_{c2} corresponds to the ellipsoidal light variations. Tidal effects make a star the brightest at phases 0.25 and 0.75, and the dimmest at phases 0.0 and 0.5. This corresponds to $a_{c2} > 0$, as the I magnitude is largest when the star is at its dimmest. The values of a_{c2} with their nominal error bars are shown in Fig. 2. Note that for a number of stars the coefficient is negative, many standard deviations smaller than zero. This clearly shows that the nominal errors are not realistic. This is understandable, as there are strong correlations between consecutive photometric data points (Kruszewski & Semeniuk 2003).

The rms deviation between the five parameter fit and the data is a measure of the photometric errors for individual measurements. The rms errors and the average of the formal errors of the four sinusoidal coefficients of the fit are shown in Fig. 3 with circles and triangles, respectively. The formal errors for the fitted parameters are approximately $N^{1/2}$ times smaller than the rms values, as expected; N is the number of photometric data points for a given star. Open symbols refer to the stars in the Galactic Center field, and filled symbols to the stars in Carina. The crosses are error estimates by Drake (2003, Table 1) for stars in the Galactic Center field. The squares will be explained later.

It is clear that the errors increase with the I magnitude, as expected. The errors are smaller for the Carina stars, as expected. Two stars, OGLE-TR-24 and OGLE-TR-58, show anomalously large rms. Inspection of their light curves shows they exhibit long term changes of about 0.015 magnitudes. The nature of this variability is not known, and we exclude these two objects from the error histogram shown in Fig. 5, discussed below. The orbital periods are not known for OGLE transits 43, 44, 45, and 46, so these stars are not considered in this paper. The following analysis was done for the remaining 117 objects. Note that objects 8 and 29 are the same star, but they are treated separately in the OGLE database, so we treat them separately here as well.

The planetary transit candidates have orbital periods in the range 0.57 – 9.2 days, which corresponds to the frequency of ellipsoidal variability in the range 0.22 – 3.5 d⁻¹. We calculated power spectra for every star as follows:

$$p_\nu = a_{c,\nu}^2 + a_{s,\nu}^2, \quad \nu = \frac{i}{250 \text{ day}}, \quad i = 1, 2, 3, \dots, 1000, \quad (2)$$

where

$$a_{c,\nu} = \frac{\sum_{k=1}^N (I_k - \langle I \rangle) \cos(2\pi\nu t_k)}{\sum_{k=1}^N \cos^2(2\pi\nu t_k)}, \quad a_{s,\nu} = \frac{\sum_{k=1}^N (I_k - \langle I \rangle) \sin(2\pi\nu t_k)}{\sum_{k=1}^N \sin^2(2\pi\nu t_k)}, \quad (3)$$

where the summation is done over all photometric data points for a given star, excluding the data points within the transits.

An example of the power spectrum is shown in Fig. 4 for OGLE-TR-5. Also shown is a power law fit to the spectrum:

$$p_{\nu,f} = p_0 \nu^{p_1}, \quad (4)$$

where the two parameters p_0 and p_1 were calculated for each star using a least squares method. The binary period for OGLE-TR-5 is given by Udalski et al. (2002a) as 0.8082 days. The arrows correspond to the orbital frequency $1/P_{\text{orb}} = 1.237 \text{ d}^{-1}$, and the expected frequency of ellipsoidal variability $2/P_{\text{orb}} = 2.475 \text{ d}^{-1}$.

We calculated power spectra for all stars, and each was fitted with its own power law. For every star and for every frequency we calculated the coefficients $a_{c,\nu}$ and $a_{s,\nu}$, as defined by eq. (3), and divided each by $b_\nu \equiv (p_{\nu,f}/2)^{1/2}$ to normalize it. A histogram of these normalized terms is shown in Fig. 5. Also shown is Gaussian distribution with unit variance; it is fairly similar to the histogram, which implies that b_ν provides a reasonable estimate of the statistical error.

Our power spectrum formula (eqs. 2 and 3) can be derived by a least squares method at each frequency. It is similar to the Lomb-Scargle (LS) periodogram formula (Lomb 1976, Scargle 1982, Press et al. 1992), but differs in several respects. Perhaps most importantly for this work, the LS periodogram does not distinguish between the sine and cosine terms. Therefore, a phase offset τ is necessary in the LS periodogram formula, but not in our power spectrum since we fit $a_{c,\nu}$ and $a_{s,\nu}$ separately. One strength of the LS periodogram is a prescription to determine the significance level of any peak in the power spectrum. However, this prescription is most useful when the resonant frequencies are unknown beforehand, and requires a knowledge of the number of effectively independent frequencies M in the power spectrum, because as M increases, the probability that spurious noise looks like genuine signals increases. However, in our case, we know the expected frequency of ellipsoidal variability beforehand, so the value of M is irrelevant for our simple analysis. As shown in Fig. 5, we are able to define an error b_ν for each value of $a_{c,\nu}$ and $a_{s,\nu}$ which is approximately Gaussian, so that the usual (68, 95, 99.7)%, etc. confidence values ‘approximately’ apply for values of $a_{c,\nu}$ and $a_{s,\nu}$ within $(1, 2, 3)\sigma$, etc. In other words, a value of a_{c2} that is 3σ away from zero indicates ellipsoidal variability at a 99.7% confidence level, depending on how much faith one puts into the Gaussian nature of Fig. 5. Note that the tails of the distribution are exaggerated on the logarithmic axis, and that some contribution to the tails should be from genuine signal.

For every star we calculated the a_{c1} and a_{c2} terms of eq. (1) and estimated their errors b_1 and b_2 as b_ν evaluated at the corresponding frequencies. The errors for the a_{c2} term, b_2 ,

are shown in Fig. 3 as squares. It is clear that these statistical errors are much larger than the errors shown as triangles, which were based on the assumption that all photometric data points are uncorrelated. The ‘triangle’ error bars were used in our Fig. 2, which provided the first hint that they are underestimates of the true errors, as so many values of the ellipsoidal variability parameter a_{c2} were negative with very small ‘triangle’ error bars.

The two amplitudes a_{c2} and a_{c1} are shown in Fig. 6 and Fig. 7, respectively, as a function of orbital period. Negative values of a_{c2} are physically meaningless, and presumably these are $a_{c2} \approx 0$ which were ‘scattered’ to negative values by statistical errors. Indeed, there are 29 negative values, with 20 within one σ of zero, and 9 outside of one σ , with the ratio 20/9 close to that expected for a Gaussian distribution. This also implies that our error estimate is realistic; here and in the following we take $\sigma = b_1$ for a_{c1} and a_{s1} , $\sigma = b_2$ for a_{c2} and a_{s2} .

We expect that about the same number, 29, of positive a_{c2} values is due to errors, while the remaining $117 - 29 - 29 = 59$ are real ellipsoidal variables. This estimate suggests that $\sim 50\%$ of all OGLE transit candidates have massive companions, not planets. Tidal effects responsible for ellipsoidal variations increase strongly with reduced orbit size, and therefore they are expected to be more common at short orbital periods. Indeed, this appears to be the case in Fig. 6.

Ellipsoidal variability scales with the mass ratio, and for low mass companions like planets it becomes much smaller than our errors. Hence, all OGLE transit stars with measurable ellipsoidal variability should be excluded from the list of planetary candidates. Note that blending with non-variable stars dilutes the variable component, and may suppress the amplitude of the apparent ellipsoidal variability.

Some stars vary with the orbital period. Positive values of a_{c1} , as shown in Fig. 7, may indicate a heating (reflection) effect of the companion by the primary, as in the well known case of Algol, or they may indicate that the true orbital period is twice longer than listed by OGLE, and the variability is ellipsoidal. In the former case nothing can be said about the companion mass; in the latter case the companion is too massive to be a planet.

Note that there are 44 stars in Fig. 7 with negative values of a_{c1} , and 27 of these are within their 1σ error bars of zero. This is consistent with no credible negative a_{c1} . As the errors are expected to be symmetric there must be ~ 44 stars which nominally have positive values of a_{c1} , but in fact are consistent with $a_{c1} = 0$. Unfortunately, we cannot point to the remaining 29 stars which may have real ‘reflection’ effects, except for OGLE-TR-39, which has the orbital period given as 0.8 days, and it obviously has $a_{c1} > 0$. This star shows large values (in terms of their errors) of both terms: a_{c1} and a_{c2} . This indicates that the orbital period is correct, the companion has its hemisphere facing the primary noticeably heated,

and its mass is large enough to induce ellipsoidal light variations. The reflection effect is expected to be stronger for binaries with small separations, i.e. short orbital period. There is some evidence for this effect in Fig. 7.

Table 1 lists all OGLE transit candidates with known orbital periods, giving their OGLE-TR number, average magnitude $\langle I \rangle$, orbital period P_{orb} in days, the a_{c1} and a_{c2} coefficients in milli-magnitudes, and the number of transits detected by OGLE, N_{tr} . Objects with few detected transits are more likely to have incorrect periods. Therefore, the ellipsoidal variability of the objects with $N_{\text{tr}} \sim 2$ is more likely to go undetected in our analysis (but possibly could be detected in the a_{c1} term if the incorrect period happened to be half the true period). The a_{c1} and a_{c2} coefficients are expressed in terms of their errors in Table 1, in the format $b_i(a_{ci}/b_i \pm 1)$, so that objects with larger values of a_{c2}/b_2 are more likely to be ellipsoidal variable, and those with smaller or negative values are better planetary system candidates. It should become possible to recognize more objects with bona fide ellipsoidal light variations when the systematic errors are reduced by a more thorough analysis carried out by Kruszewski & Semeniuk (2003).

It is interesting to plot a_{c1} versus a_{c2} , as shown in Fig. 8. It is clear that while there are several possibly real positive a_{c1} terms, there are considerably more positive a_{c2} terms.

In a simple model where the presence of a companion may give rise to ellipsoidal light variations and the ‘reflection’ effect the terms a_{s1} and a_{s2} in eq. (1) should be zero. Fig. 9 presents these coefficients in units of their errors. There are 29 stars with a_{s2} having absolute value larger than one σ , with 88 values smaller than one σ . The corresponding numbers for a_{s1} are 41 and 76, respectively. This is close to the ratio expected if the true values of both coefficients were zero, and their errors were Gaussian. The average and the rms values are: $\langle a_{s1}/b_1 \rangle = -0.27$, $\langle a_{s2}/b_2 \rangle = +0.10$, $\langle (a_{s1}/b_1)^2 \rangle^{1/2} = 1.17$, and $\langle (a_{s2}/b_2)^2 \rangle^{1/2} = 0.93$. All this implies that our error estimate is reasonable. Note that OGLE-TR-68, with $a_{s1}/b_1 = -4.4$, may have a real variability, possibly induced by a spot on the star.

By treating the duplicate objects OGLE-TR-8 and OGLE-TR-29 separately in this analysis, we are able to verify the consistency of the algorithm. As can be seen from Table 1, for these two objects the cosine coefficients a_{c1} and a_{c2} are consistent within error. Furthermore, for OGLE-TR-8, $a_{s1} = -0.006 \pm 1.47$, $a_{s2} = 0.643 \pm 1.32$, and for OGLE-TR-29, $a_{s1} = -0.550 \pm 1.71$, $a_{s2} = 0.664 \pm 1.55$, so the sine coefficients are also consistent within error.

3. Discussion

It is interesting to compare our errors, given in Table 1, with those estimated by Drake (2003, Table 1, Galactic Center region only). Our errors are also shown in Fig. 3 as squares, while Drake’s errors are shown with crosses. For the faintest stars systematic errors are comparable to the photon noise, hence there is only a small difference, approximately a factor of 2. For the bright stars photon noise is negligible compared to systematic errors, and our estimate is up to 5 times larger than Drake’s (OGLE-TR-16). We stress that our estimate is realistic, as demonstrated with Fig. 8 and Fig. 9. Consider as an example OGLE-TR-5, with its spectrum shown in Fig. 4. The peak corresponding to the ellipsoidal variability at $2/P_{\text{orb}} = 2.48 \text{ d}^{-1}$ is strong and certainly real. The amplitude is $a_{e2} = 7.5 \text{ mmag}$ in our Table 1, and 7.2 mmag in Drake’s Table 1. However, the errors are 1.3 mmag and 0.4 mmag , respectively. The power spectrum presented in Fig. 4 clearly shows a high level of noise, which is used for our error estimate.

In the case of OGLE-TR-5 the ellipsoidal variability is highly significant with either of the two error estimates. It is not so with OGLE-TR-40, which is listed by Drake as being ellipsoidal variable at the 3.5σ level, while our analysis puts it at just a one σ level, i.e. nothing definite can be said about this case.

The star with the first planetary companion confirmed spectroscopically, OGLE-TR-56 (Konacki et al. 2003), should not have a measurable value of a_{e2} , and reassuringly we do not detect a significant ellipsoidal variability (cf. Table 1). The planetary disk covers $\sim 2 \times 10^{-4}$ of the sky as seen from the star, i.e. the reflection effect has to be small, $a_{e1} < 0.1 \text{ mmag}$. The measured value is $a_{e1} = 1.08 \pm 0.46 \text{ mmag}$, and presumably it is not significant.

A thorough analysis of various systematic effects apparent in the photometry of tens of thousands of variable and non-variable stars measured in the OGLE fields is currently being done by Kruszcwski & Semeniuk (2003). Preliminary results indicate that various systematic errors may be reduced considerably. This may allow a detection of smaller ellipsoidal effects than we could find, and may provide a cleaner list of systems which are likely to have planetary companions. At this time spectroscopists may use our Table 1 to select stars for their planetary search, eliminating objects with measurable ellipsoidal variability, as it implies a large mass ratio, and most likely a red dwarf companion.

If the objective of this work was to identify stars with definite ellipsoidal variability, we would select stars with their a_{e2} terms positive at the several σ level. But our objective is different: we identify stars which are the best candidates to have planetary companions, i.e. stars without ellipsoidal variability. This can be done in a statistical sense only. The best candidates are those for which the a_{e2} term is either negative or positive but small. However,

even if we had perfect statistical information we could only assign a probability that a given star does or does not have ellipsoidal variability. This would always be in the sense that the smaller the a_{c2} term relative to its error, the more likely the star is a planetary system. Given limited access to big telescopes needed for spectroscopic follow-up it is best to study the stars with the smallest (i.e., negative) a_{c2} terms first, and gradually move ‘up’ in a_{c2}/b_2 from Table 1.

There are several developments which will improve the situation gradually. First, OGLE continues its ‘planetary campaigns’ and new candidate stars will be published periodically. Second, a highly improved analysis of photometry is under way (Kruszewski & Semeniuk 2003), which will reduce the correlation of consecutive photometric data points considerably. This will allow a detection of smaller amplitude ellipsoidal variations, and a much better rejection of stars with non-planetary companions. It will also be possible to identify stars with even smaller depth of transits, extending the current list.

It is a pleasure to acknowledge many useful suggestions and discussions with A. Kruszewski, R. Lupton, S. Ruciński and A. Udalski. We thank the referee for many useful suggestions and for identifying the star with two names. This research was supported by the NASA grant NAG5-12212 and the NSF grant AST-0204908.

REFERENCES

- Charbonneau, D., Brown, T. M., Latham, D. W., & Mayor, M. 2000, *ApJ*, 529, L45
- Drake, A. J. 2003, *astro-ph/0301295*
- Henry, G. W., Marcy, G. W., Butler, R. P., & Vogt, S. S. 2000, *ApJ*, 529, L41
- Horne, K. 2003, *astro-ph/0301250*
- Konacki, M., Torres, G., Jha, S., & Sasselov, D. D. 2003, *Nature*, 421, 507
- Kruszewski, A., & Semeniuk, I. 2003, in preparation
- Lomb, N. R. 1976, *Ap&SS*, 39, 447
- Mazeh, T., Naef, D., Torres, G., Latham, D. W., Mayor, M. et al. 2000, *ApJ*, 532, L55
- Press, W. H., Flannery, B. P., Teukolsky, S. A., & Vetterling, W. T. 1992, *Numerical Recipes*.
Cambridge Univ. Press, Cambridge
- Scargle, J. D. 1982, *ApJ*, 263, 835
- Shobbrook, R. R., Herbison-Evans, D., Johnston, I. D., & Lomb, N. R. 1969, *MNRAS*, 145,

Udalski, A., Paczyński, B., Zebruń, K., Szymański, M., Kubiak, M. et al. 2002, *AcA*, 52, 1
Udalski, A., Zebruń, K., Szymański, M., Kubiak, M., Soszyński, I. et al. 2002, *AcA*, 52, 115
Udalski, A., Szewczyk, O., Zebruń, K., Pietrzyński, G., Szymański, M. et al. 2002, *AcA*, 52,
317

Table 1. List of transiting objects

Object name	$\langle I \rangle$	P_{orb}	a_{c1}	a_{c2}	N_{tr}
OGLE-TR-1	15.655	1.601	0.92 (+1.27 ± 1)	0.86 (−0.28 ± 1)	4
OGLE-TR-2	14.173	2.813	0.83 (−1.36 ± 1)	0.76 (+3.78 ± 1)	5
OGLE-TR-3	15.564	1.189	0.73 (+3.54 ± 1)	0.67 (+3.96 ± 1)	14
OGLE-TR-4	14.714	2.619	1.24 (+0.01 ± 1)	1.15 (+0.24 ± 1)	5
OGLE-TR-5	14.877	0.808	1.32 (+0.98 ± 1)	1.28 (+5.87 ± 1)	8
OGLE-TR-6	15.351	4.549	1.36 (+3.54 ± 1)	1.25 (+2.40 ± 1)	4
OGLE-TR-7	14.795	2.718	1.18 (+0.66 ± 1)	1.05 (+1.79 ± 1)	5
OGLE-TR-8*	15.647	2.715	1.47 (+1.70 ± 1)	1.32 (+1.53 ± 1)	4
OGLE-TR-9	14.010	3.269	0.82 (+0.47 ± 1)	0.73 (+1.05 ± 1)	4
OGLE-TR-10	14.928	3.101	1.05 (−0.97 ± 1)	0.93 (+1.38 ± 1)	7
OGLE-TR-11	16.007	1.615	0.80 (+0.05 ± 1)	0.74 (+2.23 ± 1)	7
OGLE-TR-12	14.673	5.772	0.83 (+0.20 ± 1)	0.77 (−1.79 ± 1)	2
OGLE-TR-13	13.893	5.853	0.75 (+0.74 ± 1)	0.67 (+2.12 ± 1)	2
OGLE-TR-14	13.064	7.798	0.71 (−0.25 ± 1)	0.65 (+2.71 ± 1)	3
OGLE-TR-15	13.228	4.875	0.98 (−1.91 ± 1)	0.90 (−0.13 ± 1)	4
OGLE-TR-16	13.509	2.139	1.92 (+0.26 ± 1)	1.70 (+8.31 ± 1)	4
OGLE-TR-17	16.217	2.317	0.94 (+0.78 ± 1)	0.89 (+1.13 ± 1)	4
OGLE-TR-18	16.006	2.228	0.81 (+1.32 ± 1)	0.75 (+5.74 ± 1)	6
OGLE-TR-19	16.352	5.282	1.12 (−0.67 ± 1)	1.01 (+0.21 ± 1)	2
OGLE-TR-20	15.407	4.284	1.14 (+0.10 ± 1)	1.04 (+0.55 ± 1)	3
OGLE-TR-21	15.585	6.893	0.70 (+0.02 ± 1)	0.65 (+2.93 ± 1)	3
OGLE-TR-22	14.549	4.275	1.39 (−3.07 ± 1)	1.25 (−0.23 ± 1)	3
OGLE-TR-23	16.396	3.287	1.11 (−2.41 ± 1)	1.04 (−0.58 ± 1)	2
OGLE-TR-24	14.843	5.282	2.63 (+0.78 ± 1)	2.20 (+1.11 ± 1)	2
OGLE-TR-25	15.274	2.218	1.06 (+0.21 ± 1)	0.98 (+3.29 ± 1)	5
OGLE-TR-26	14.784	2.539	1.09 (−0.16 ± 1)	0.93 (−0.25 ± 1)	4
OGLE-TR-27	15.712	1.715	1.34 (−0.23 ± 1)	1.25 (+5.61 ± 1)	6
OGLE-TR-28	16.436	3.405	0.96 (−1.36 ± 1)	0.87 (−1.97 ± 1)	3
OGLE-TR-29*	15.646	2.716	1.71 (+1.96 ± 1)	1.55 (+0.88 ± 1)	4
OGLE-TR-30	14.923	2.365	0.67 (+0.43 ± 1)	0.60 (+3.36 ± 1)	6
OGLE-TR-31	14.332	1.883	0.86 (−0.12 ± 1)	0.75 (+5.16 ± 1)	7

Table 1—Continued

Object name	$\langle I \rangle$	P_{orb}	a_{c1}	a_{c2}	N_{tr}
OGLE-TR-32	14.849	1.343	0.95 (+1.07 ± 1)	0.87 (+7.18 ± 1)	7
OGLE-TR-33	13.716	1.953	0.99 (−0.84 ± 1)	0.93 (−2.31 ± 1)	4
OGLE-TR-34	15.997	8.581	0.42 (−2.25 ± 1)	0.42 (+0.41 ± 1)	3
OGLE-TR-35	13.264	1.260	0.93 (+4.26 ± 1)	0.85 (+0.99 ± 1)	7
OGLE-TR-36	15.767	6.252	1.23 (−0.56 ± 1)	1.08 (+0.23 ± 1)	2
OGLE-TR-37	15.183	5.720	0.98 (+0.75 ± 1)	0.90 (−0.84 ± 1)	2
OGLE-TR-38	14.675	4.101	0.88 (−1.21 ± 1)	0.82 (−0.23 ± 1)	3
OGLE-TR-39	14.674	0.815	1.12 (+7.43 ± 1)	1.07 (+5.03 ± 1)	11
OGLE-TR-40	14.947	3.431	0.81 (+0.57 ± 1)	0.72 (+1.00 ± 1)	5
OGLE-TR-41	13.488	4.517	0.62 (+0.28 ± 1)	0.56 (−0.49 ± 1)	2
OGLE-TR-42	15.395	4.161	0.65 (−0.07 ± 1)	0.60 (+0.52 ± 1)	4
OGLE-TR-47	15.604	2.336	0.78 (+1.26 ± 1)	0.71 (+0.65 ± 1)	7
OGLE-TR-48	14.771	7.226	0.99 (−1.16 ± 1)	0.95 (+0.21 ± 1)	2
OGLE-TR-49	16.181	2.690	0.80 (+0.88 ± 1)	0.79 (−1.53 ± 1)	2
OGLE-TR-50	15.923	2.249	0.86 (−0.16 ± 1)	0.77 (+0.51 ± 1)	3
OGLE-TR-51	16.716	1.748	0.67 (+1.13 ± 1)	0.71 (−0.32 ± 1)	5
OGLE-TR-52	15.593	1.326	1.24 (+0.58 ± 1)	1.16 (+3.20 ± 1)	8
OGLE-TR-53	16.000	2.906	0.72 (−0.06 ± 1)	0.68 (+1.41 ± 1)	4
OGLE-TR-54	16.473	8.163	1.20 (+1.78 ± 1)	1.08 (−0.65 ± 1)	3
OGLE-TR-55	15.803	3.185	0.82 (−0.74 ± 1)	0.75 (+0.19 ± 1)	6
OGLE-TR-56	15.300	1.212	0.46 (+2.33 ± 1)	0.43 (−1.35 ± 1)	11
OGLE-TR-57	15.695	1.675	1.01 (+0.73 ± 1)	0.95 (+6.49 ± 1)	5
OGLE-TR-58	14.754	4.345	2.45 (−1.03 ± 1)	2.15 (−1.43 ± 1)	3
OGLE-TR-59	15.195	1.497	0.81 (+3.37 ± 1)	0.76 (+2.49 ± 1)	9
OGLE-TR-60	14.601	2.309	0.42 (+1.07 ± 1)	0.32 (+4.32 ± 1)	11
OGLE-TR-61	16.258	4.268	1.18 (+0.73 ± 1)	1.11 (+7.77 ± 1)	8
OGLE-TR-62	15.907	2.601	0.67 (+2.02 ± 1)	0.61 (+5.07 ± 1)	10
OGLE-TR-63	15.751	1.067	0.47 (+0.17 ± 1)	0.43 (−0.59 ± 1)	12
OGLE-TR-64	16.169	2.717	0.51 (+0.74 ± 1)	0.49 (+0.85 ± 1)	7
OGLE-TR-65	15.941	0.860	0.55 (+4.29 ± 1)	0.51 (−1.00 ± 1)	18
OGLE-TR-66	15.180	3.514	0.56 (−1.44 ± 1)	0.54 (+2.05 ± 1)	6

Table 1—Continued

Object name	$\langle I \rangle$	P_{orb}	a_{c1}	a_{c2}	N_{tr}
OGLE-TR-67	16.399	5.280	0.87 (+1.59 ± 1)	0.74 (+2.40 ± 1)	5
OGLE-TR-68	16.793	1.289	1.17 (+0.53 ± 1)	1.12 (+2.15 ± 1)	12
OGLE-TR-69	16.550	2.337	0.74 (+2.58 ± 1)	0.69 (+2.14 ± 1)	5
OGLE-TR-70	16.890	8.041	0.64 (−1.31 ± 1)	0.61 (+0.12 ± 1)	4
OGLE-TR-71	16.379	4.188	0.50 (−3.74 ± 1)	0.46 (+2.11 ± 1)	5
OGLE-TR-72	16.440	6.854	1.32 (+1.13 ± 1)	1.16 (+0.20 ± 1)	4
OGLE-TR-73	16.989	1.581	0.97 (+3.61 ± 1)	0.86 (−0.32 ± 1)	9
OGLE-TR-74	15.869	1.585	1.11 (+0.52 ± 1)	0.99 (+0.56 ± 1)	11
OGLE-TR-75	16.964	2.643	0.69 (+0.65 ± 1)	0.66 (+3.73 ± 1)	8
OGLE-TR-76	13.760	2.127	0.66 (+0.04 ± 1)	0.61 (+1.47 ± 1)	6
OGLE-TR-77	16.122	5.455	0.53 (+0.48 ± 1)	0.47 (−0.16 ± 1)	4
OGLE-TR-78	15.319	5.320	0.37 (−0.96 ± 1)	0.32 (+2.00 ± 1)	4
OGLE-TR-79	15.277	1.325	0.45 (+0.04 ± 1)	0.44 (+10.13 ± 1)	13
OGLE-TR-80	16.501	1.807	0.77 (+2.81 ± 1)	0.71 (+4.83 ± 1)	12
OGLE-TR-81	15.413	3.216	0.96 (−0.12 ± 1)	0.86 (+2.76 ± 1)	6
OGLE-TR-82	16.304	0.764	0.84 (+0.28 ± 1)	0.69 (+0.85 ± 1)	22
OGLE-TR-83	14.865	1.599	0.71 (+2.40 ± 1)	0.66 (+8.11 ± 1)	12
OGLE-TR-84	16.692	3.113	0.68 (−0.24 ± 1)	0.64 (+2.01 ± 1)	6
OGLE-TR-85	15.452	2.115	0.53 (−0.50 ± 1)	0.41 (+2.83 ± 1)	12
OGLE-TR-86	16.319	2.777	0.89 (+1.90 ± 1)	0.80 (+1.19 ± 1)	7
OGLE-TR-87	16.321	6.607	0.61 (−0.71 ± 1)	0.56 (−0.35 ± 1)	3
OGLE-TR-88	14.578	1.250	0.67 (+1.70 ± 1)	0.62 (+5.20 ± 1)	15
OGLE-TR-89	15.782	2.290	0.40 (+1.13 ± 1)	0.36 (+0.09 ± 1)	5
OGLE-TR-90	16.441	1.042	0.60 (−1.09 ± 1)	0.56 (+2.69 ± 1)	15
OGLE-TR-91	15.231	1.579	1.20 (+0.35 ± 1)	1.16 (+5.65 ± 1)	9
OGLE-TR-92	16.496	0.978	0.56 (−0.37 ± 1)	0.50 (+6.55 ± 1)	20
OGLE-TR-93	15.198	2.207	0.62 (+0.46 ± 1)	0.57 (+5.47 ± 1)	12
OGLE-TR-94	14.319	3.092	0.54 (+0.81 ± 1)	0.48 (+4.16 ± 1)	6
OGLE-TR-95	16.366	1.394	0.89 (−2.80 ± 1)	0.83 (+3.12 ± 1)	14
OGLE-TR-96	14.900	3.208	0.56 (−0.00 ± 1)	0.47 (−0.10 ± 1)	6
OGLE-TR-97	15.512	0.568	0.67 (+1.18 ± 1)	0.63 (+1.72 ± 1)	25

Table 1—Continued

Object name	$\langle I \rangle$	P_{orb}	a_{c1}	a_{c2}	N_{tr}
OGLE-TR-98	16.639	6.398	0.47 (+0.63 ± 1)	0.45 (−0.35 ± 1)	5
OGLE-TR-99	16.469	1.103	0.65 (+1.86 ± 1)	0.57 (+5.47 ± 1)	16
OGLE-TR-100	14.879	0.827	0.85 (+1.11 ± 1)	0.81 (+2.83 ± 1)	20
OGLE-TR-101	16.689	2.362	0.78 (−0.10 ± 1)	0.70 (+3.88 ± 1)	8
OGLE-TR-102	13.841	3.098	0.33 (−2.05 ± 1)	0.30 (+1.32 ± 1)	5
OGLE-TR-103	16.694	8.217	0.42 (−0.98 ± 1)	0.42 (−1.45 ± 1)	4
OGLE-TR-104	17.099	6.068	0.68 (−0.40 ± 1)	0.64 (−0.19 ± 1)	2
OGLE-TR-105	16.160	3.058	1.00 (+0.98 ± 1)	0.85 (−0.69 ± 1)	3
OGLE-TR-106	16.529	2.536	0.89 (+1.49 ± 1)	0.77 (+1.30 ± 1)	6
OGLE-TR-107	16.664	3.190	0.84 (−1.08 ± 1)	0.74 (+0.15 ± 1)	7
OGLE-TR-108	17.282	4.186	0.94 (+0.20 ± 1)	0.88 (+2.15 ± 1)	3
OGLE-TR-109	14.990	0.589	0.35 (+2.22 ± 1)	0.33 (+1.85 ± 1)	24
OGLE-TR-110	16.149	2.849	0.51 (+1.00 ± 1)	0.47 (+1.27 ± 1)	6
OGLE-TR-111	15.550	4.016	0.45 (+0.05 ± 1)	0.41 (−0.64 ± 1)	9
OGLE-TR-112	13.641	3.879	0.43 (+1.52 ± 1)	0.37 (+3.32 ± 1)	8
OGLE-TR-113	14.422	1.433	0.45 (−1.61 ± 1)	0.39 (−1.79 ± 1)	10
OGLE-TR-114	15.763	1.712	0.86 (+0.35 ± 1)	0.79 (−1.20 ± 1)	5
OGLE-TR-115	16.658	8.347	0.60 (+0.97 ± 1)	0.57 (+0.22 ± 1)	3
OGLE-TR-116	14.899	6.064	1.00 (−0.34 ± 1)	0.77 (+0.41 ± 1)	5
OGLE-TR-117	16.710	5.023	0.67 (−0.29 ± 1)	0.62 (+1.15 ± 1)	5
OGLE-TR-118	17.073	1.861	0.63 (+1.24 ± 1)	0.59 (+2.00 ± 1)	7
OGLE-TR-119	14.291	5.283	0.92 (−0.12 ± 1)	0.74 (+1.18 ± 1)	7
OGLE-TR-120	16.229	9.166	0.63 (−0.73 ± 1)	0.57 (+0.60 ± 1)	4
OGLE-TR-121	15.861	3.232	0.71 (−0.30 ± 1)	0.60 (+3.06 ± 1)	6

Note. — We present the a_{c1} and a_{c2} coefficients in the format $b_i(a_{ci}/b_i \pm 1)$ to more easily identify the ratio of the coefficients to their errors. *OGLE-TR-8 and OGLE-TR-29 are the same object, but recorded as two separate events by OGLE. We treat them separately throughout this paper.

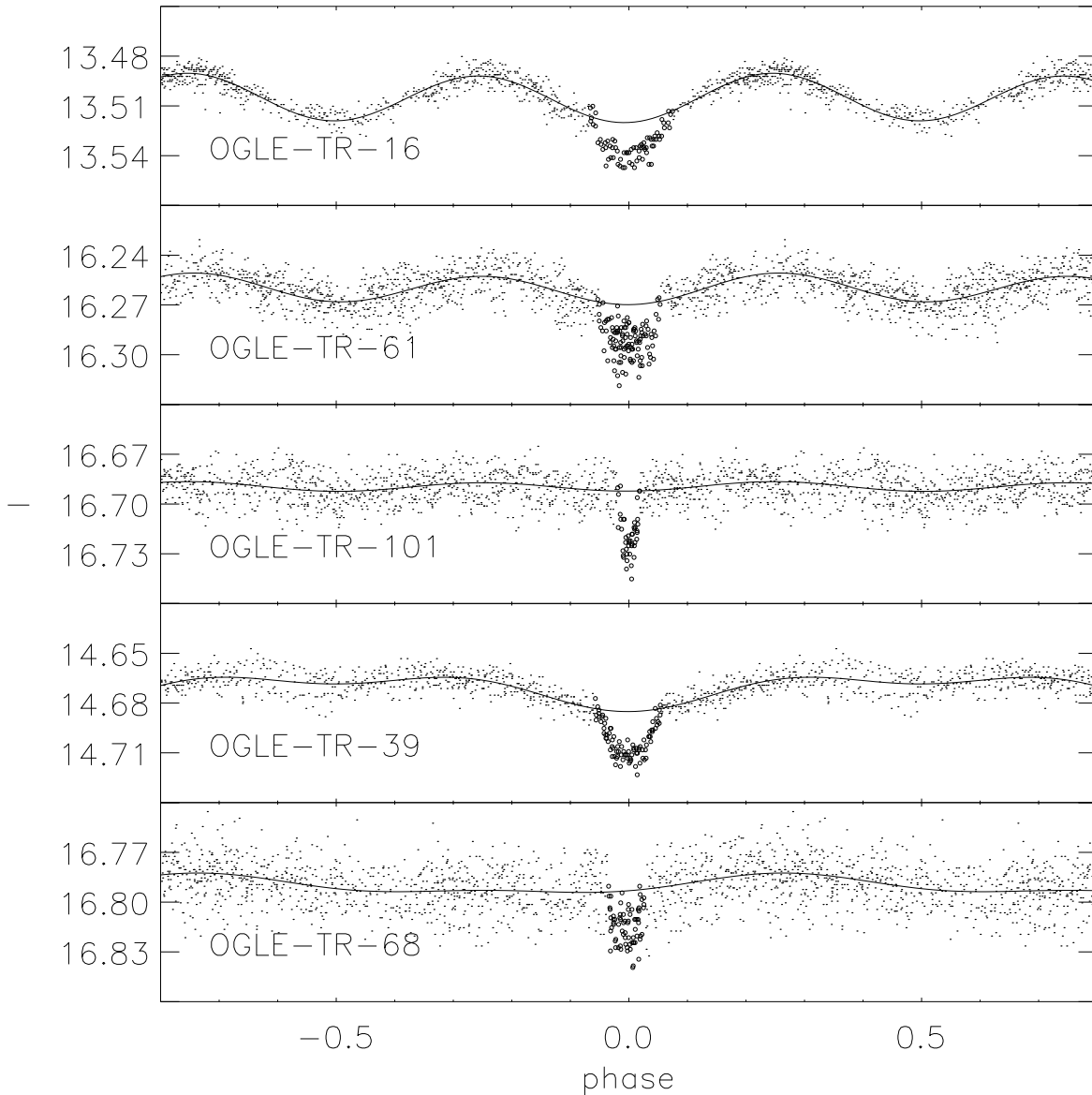


Fig. 1.— Light curves of five transiting objects, folded with the transit at zero phase, are shown as examples. Photometric data points within the transits, indicated with circles, are not used in fitting. The best-fit five-parameter function (eq. 1) is also plotted. Objects OGLE-TR-16 and TR-61 have ellipsoidal variability at about the 8σ level, while OGLE-TR-101 has ellipsoidal variability at about a 4σ level (cf. Table 1). OGLE-TR-39 has a strong a_{e1} term, indicative of surface heating (cf. Fig. 7 and 8), as well as a strong ellipsoidal variability term a_{e2} . OGLE-TR-68 has a strong a_{s1} term (cf. Fig. 9), indicating a probable spot activity.

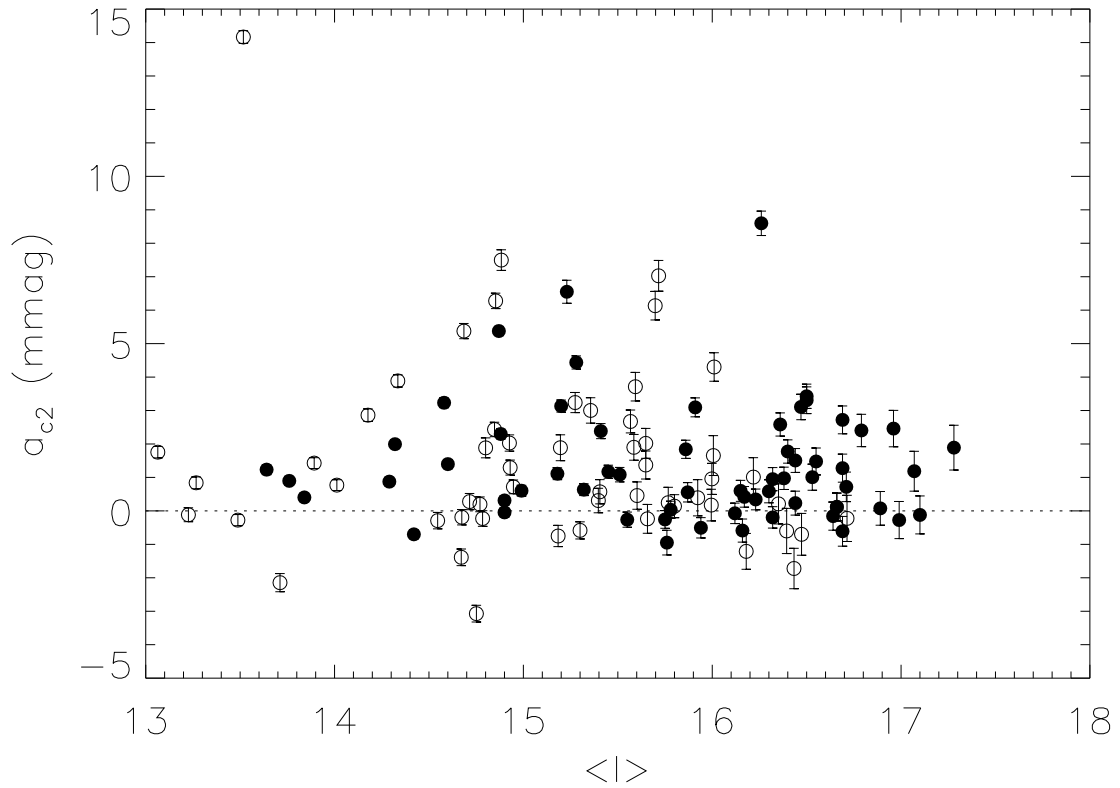


Fig. 2.— The values of the parameter corresponding to ellipsoidal light variations are shown as a function of average stellar magnitude $\langle I \rangle$. Open and filled symbols refer to the data sets OGLE-TR-1 to TR-59 and TR-60 to TR-121, respectively. Formal errors obtained with the least squares fit are also shown. Note a number of stars with negative, i.e. not physical, values of a_{c2} , which are many formal standard deviations below zero. This indicates that the errors are not realistic.

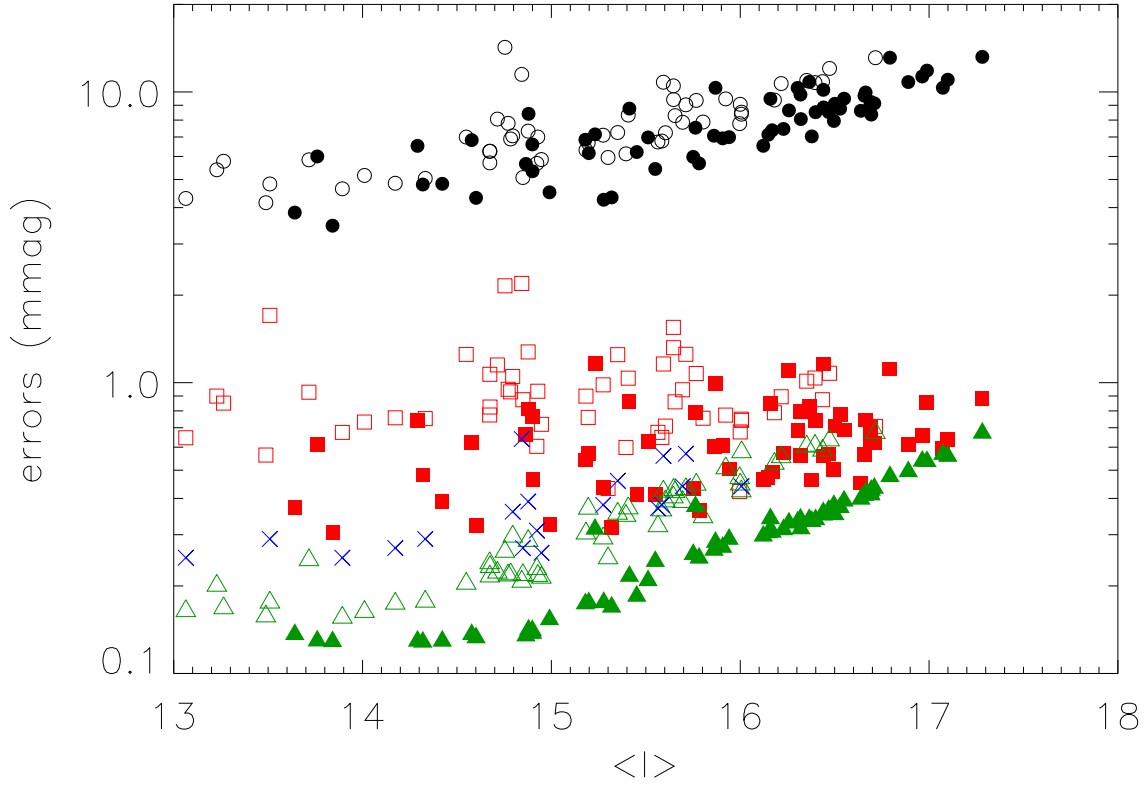


Fig. 3.— Photometric errors are shown as a function of $\langle I \rangle$ magnitude. Circles refer to the errors of individual data points, defined as an rms deviation from a 5 parameter fit to the light curves outside of the transits (cf. eq. 1). The two outliers near $\langle I \rangle \approx 14.8$, stars TR-24 and TR-58, have a long term variability at the level of 0.015 mag. Triangles are the average of the formal errors of the 5 parameter fit obtained with the least squares solution of eq. (1). Squares are the errors of the a_{c2} term determined with our spectral analysis - note they are considerably larger than the formal errors, as the photometric data have a strong time correlation. Open and filled symbols refer to the OGLE-TR-1 to TR-59 and TR-60 to TR-121 data sets, respectively. Errors listed by Drake (2003) in his Table 1 are shown with crosses for stars in the Galactic Center region.

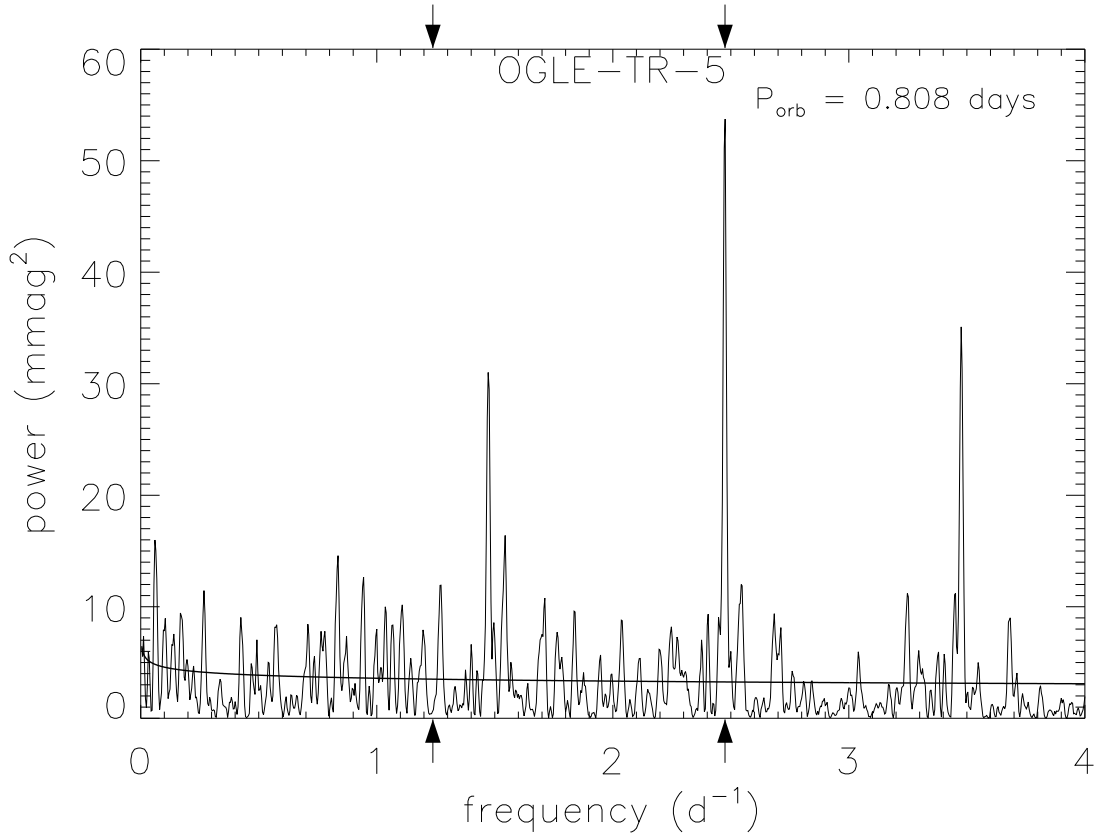


Fig. 4.— The power spectrum is shown for OGLE-TR-5. The thick solid line is the least squares power law fit to the spectrum. The two arrows correspond to the orbital frequency $1/P_{\text{orb}} = 1.237 \text{ d}^{-1}$, and the frequency of expected ellipsoidal variability $2/P_{\text{orb}} = 2.475 \text{ d}^{-1}$. Notice a very strong peak at the ‘ellipsoidal’ frequency, and the two aliases at 1.475 d^{-1} and at 3.475 d^{-1} .

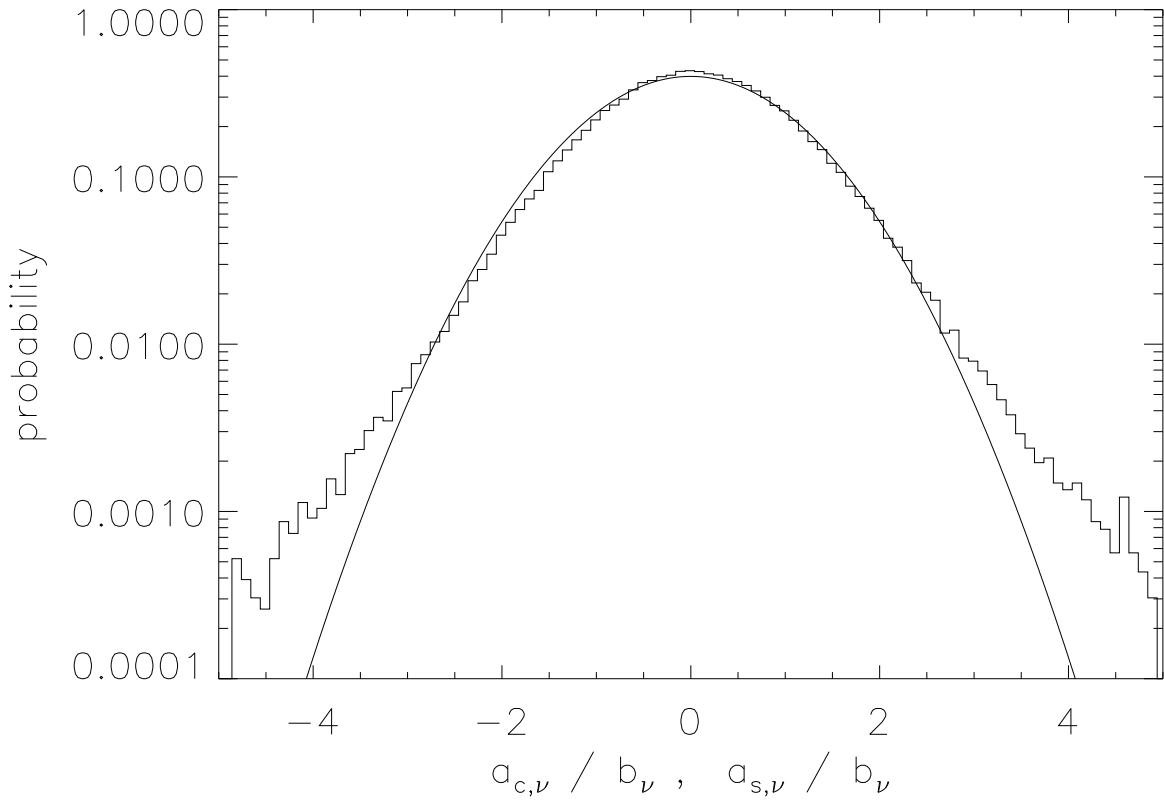


Fig. 5.— The distribution of normalized amplitudes of sine and cosine terms for all sampled frequencies and for all transit candidates except OGLE-TR-24 and TR-58. The ordinate axis is logarithmic to bring out the tails in the distribution. For comparison a Gaussian distribution with unit variance is also shown.

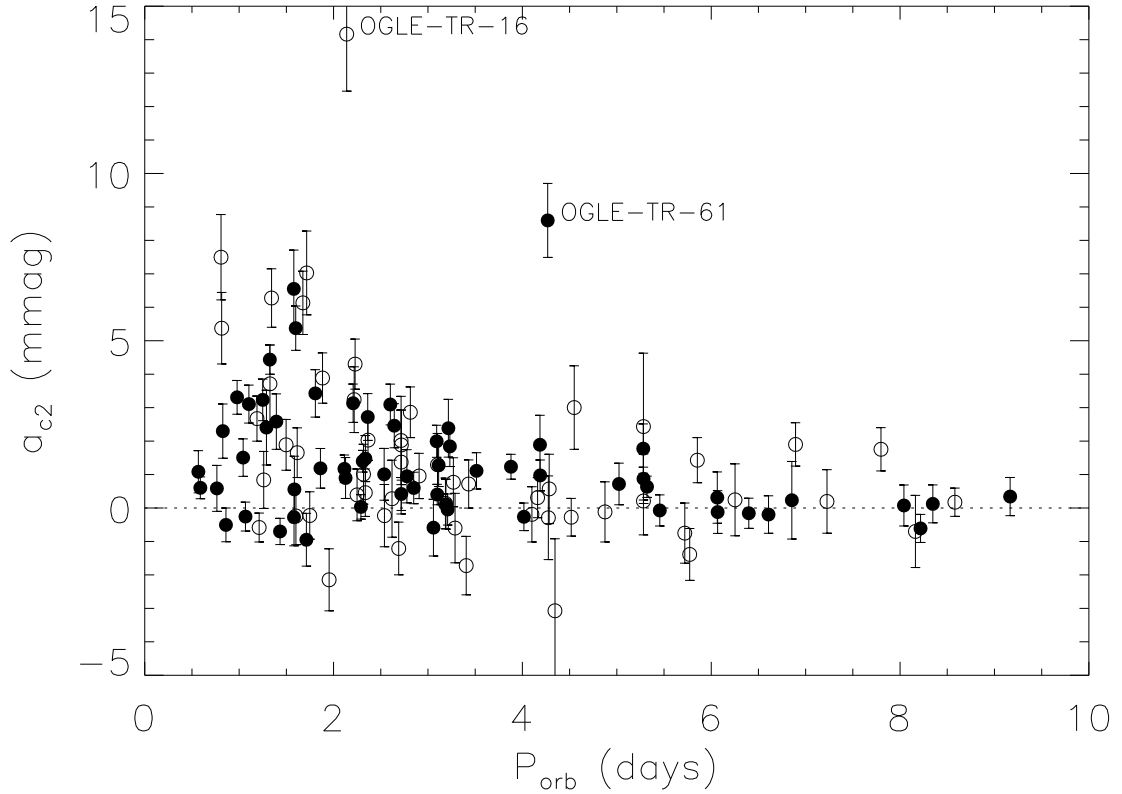


Fig. 6.— The values of the parameter a_{c2} , corresponding to ellipsoidal light variations, are shown as a function of orbital period, P_{orb} . Open and filled symbols refer to the stars OGLE-TR-1 to TR-59, and TR-60 to TR-121, respectively. The errors are based on the limited spectral analysis presented in this paper. None of the negative values are significant. Up to $\sim 50\%$ of all stars may have significant ellipsoidal variability, indicating a massive, not planetary, companion.

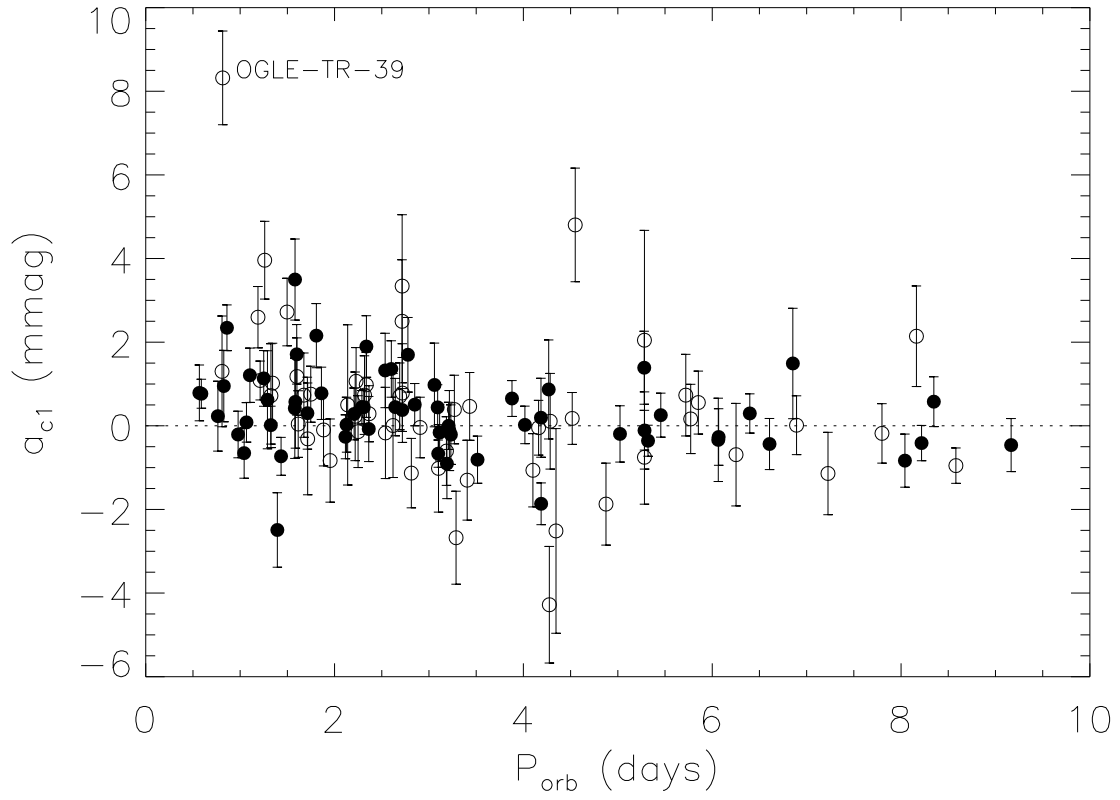


Fig. 7.— The same as Fig. 6, but for the a_{c1} parameter, which is indicative of possible ‘heating’ (reflection) effects of the companion’s hemisphere facing the primary. Only OGLE-TR-39 shows the effect strongly, but there may be several other stars for which the effect is real.

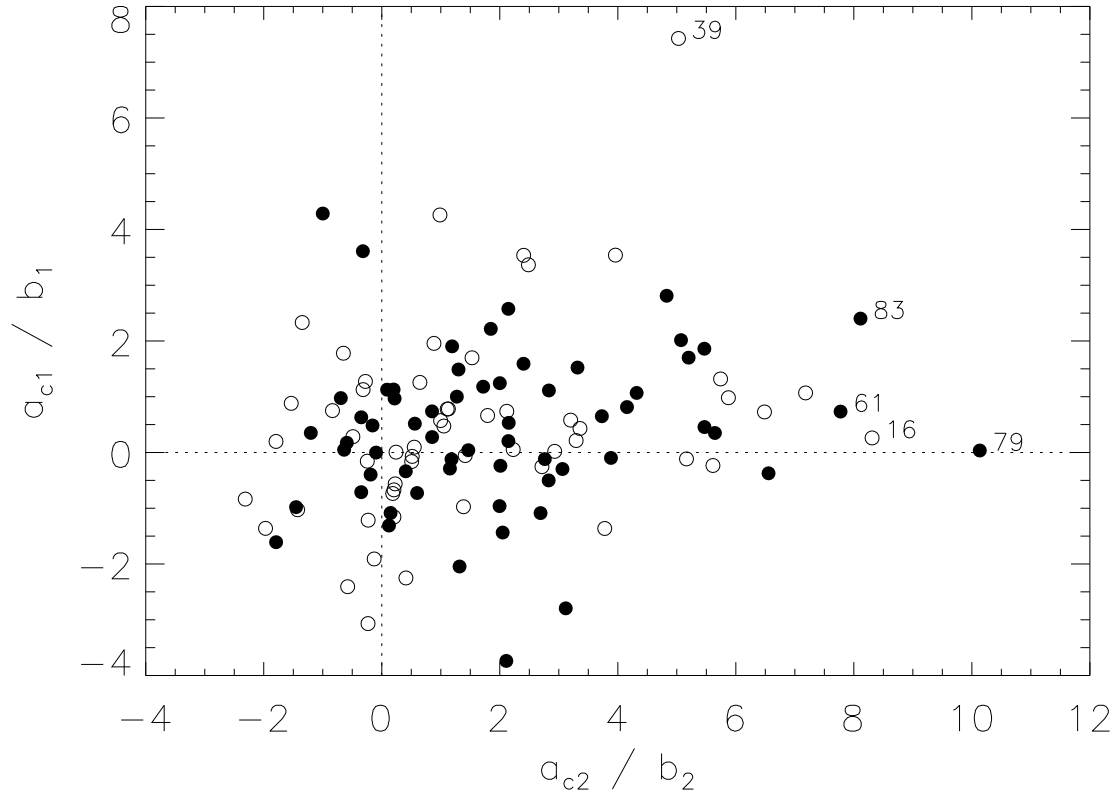


Fig. 8.— A relation between the ellipsoidal variability parameter a_{c2} , and the heating variability parameter a_{c1} (cf. eq. 1), both normalized by their errors. The stars with the strongest effects are labeled with their OGLE names. The negative values of either parameter are consistent with them being due to errors.

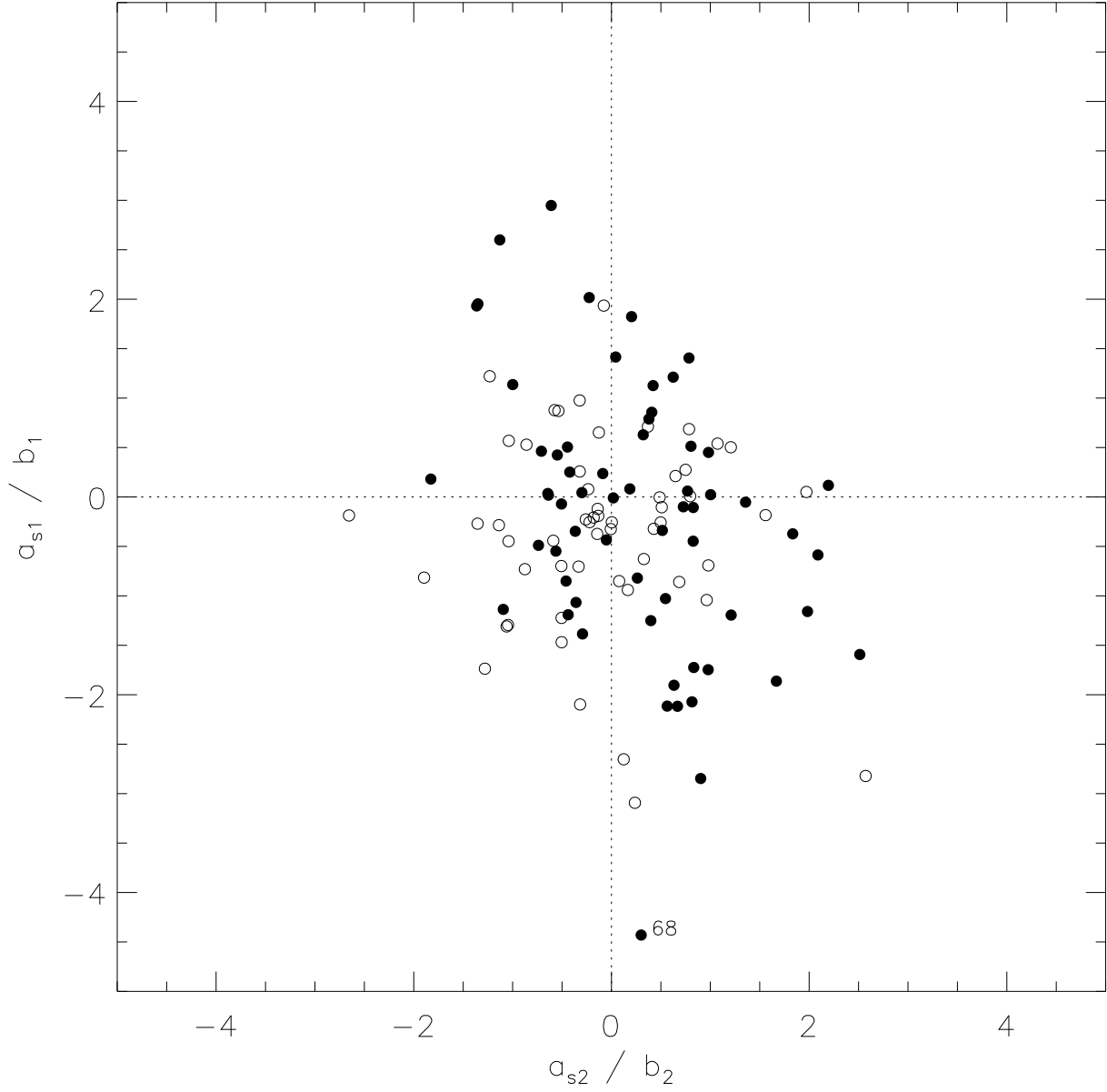


Fig. 9.— A relation between the coefficients of the sine terms in eq. (1), normalized by their errors. The ratio of the number of stars having a_{s1} within one σ of zero to the number outside of one σ is approximately 2/1, and for a_{s2} the ratio is approximately 3/1. We expect these ratios to be 2/1 if the true values are zero and the distributions are Gaussian. We conclude that our error estimate is reasonable, and we have no coefficients a_{s1} or a_{s2} that are measurably non-zero, with the possible exception of OGLE-TR-68, the filled circle with $a_{s1}/b_1 = -4.4$. Visual inspection of its light curve clearly shows that the system is approximately 15 mmag brighter at phase 0.25 than it is at phase 0.75.